Entanglement production in chaotic quantum dots subject to spin-orbit coupling

Diego Frustaglia,[1] Simone Montangero,[1] and Rosario Fazio[1,2]
[1]*NEST-CNR-INFM & Scuola Normale Superiore, I-56126 Pisa, Italy*
[2]*International School for Advanced Studies (SISSA), I-34014, Trieste, Italy*
(Received 9 May 2006; revised manuscript received 1 September 2006; published 24 October 2006)

We study numerically the production of orbital and spin entangled states in chaotic quantum dots for noninteracting electrons. The introduction of spin-orbit coupling permits us to identify signatures of time-reversal symmetry correlations in the entanglement production previously unnoticed, resembling weak-(anti)localization quantum corrections to the conductance. We find the entanglement to be strongly dependent on spin-orbit coupling, showing universal features for broken time-reversal and spin-rotation symmetries.

DOI: 10.1103/PhysRevB.74.165326 PACS number(s): 73.23.−b, 05.70.Ln, 03.67.Mn, 05.45.Pq

I. INTRODUCTION

The existence of entangled many-particle quantum states subject to nonclassical correlations is widely recognized as a fundamental resource for quantum information processing. Two quantum systems A and B are said to be entangled if they are not separable, namely, if the common (pure) state $|\Psi_{AB}\rangle$ can not be written as the product of individual states $|\Psi_A\rangle$ and $|\Psi_B\rangle$ (i.e., $|\Psi_{AB}\rangle \neq |\Psi_A\rangle|\Psi_B\rangle$). In this case the internal degrees of freedom of systems A and B are quantum mechanically correlated, since any measurement performed on system A would condition the results of a measurement on system B beyond any classical constraint. In solid-state physics, several aspects related to the production, control, and detection of entangled electronic states have been addressed (see Ref. 1 for a recent review) and an extended literature already exists.[2–25] Most of the existing proposals for the generation of electronic entanglement are based on the presence of some kind of interaction between the particles involved as, e.g., Coulomb interaction, (anti)ferromagnetism, superconducting pairing, etc. In contrast to the original belief, it was recently recognized that interactions are indeed not necessary to produce entanglement. Noninteracting electrons, initially in a separable uncorrelated state, can evolve into an entangled state due to exchange correlations in a scattering process from an external potential.[1–8] This applies to electronic transport in multiterminal mesoscopic quantum conductors. In this approach, the efficiency of the entangler depends on the particular characteristics of the scatterer, which is described by its corresponding scattering matrix S. Among the several possibilities, systems of special interest are disorder-free chaotic quantum dots, also referred to as chaotic billards. These have the advantage of allowing for a statistical analysis that can reveal universal properties of (chaotic) electronic entanglers. This case was recently addressed by Beenakker *et al.*[2] by means of a random-matrix-theory (RMT) approach. They obtained a universal mean value for the degree of two-electron entanglement produced between spatially separated orbital channels, and remarkably found that it is not significantly affected by the breaking of time-reversal symmetry (TRS)—in contrast to other (single-particle) transport characteristics such as the conductance. Later, Samuelsson, Sukhorukov, and Büttiker[5] reformulated the problem by formally including the spin, though in the absence of any spin-dependent interaction.

In this paper we study the production of both orbital and spin two-particle entanglement for noninteracting electrons in multiterminal chaotic billards. We approach the problem numerically. By introducing the Rashba spin-orbit (SO) coupling[26] together with a magnetic-flux-breaking TRS, we are able to identify the signatures of weak-localization (WL) and weak-antilocalization (WA) quantum corrections in the entanglement production. Such TRS correlation effects appear as a constraint that can limit or enhance the efficiency of the entangler. We find that the production of spin as well as orbital entanglement is strongly affected by SO coupling on a scale corresponding to the pass from WL to WA. Additionally, we show that a finite residual entanglement survives after the breaking of both TRS and spin-rotation symmetry showing some universal characteristics.

The paper is organized as follows. In Sec. II we describe our numerical model and shortly review some relevant single-particle properties as the WL and WA quantum corrections to the conductance. In Sec. III we start discussing the interaction-free production of entanglement from a separable two-particle state (Sec. III A). We introduce the concurrence as a measure of two-qubit entanglement in Sec. III C. In Sec. III B we discuss some features related to the accessible entanglement as a consequence of the local particle number conservation. The results are presented in Sec. IV, followed by a short summary of conclusions in Sec. V.

II. MODEL AND SINGLE-PARTICLE PROPERTIES

We consider a two-dimensional chaotic dot connected to electron reservoirs at the left and right, as shown in Fig. 1.[28]

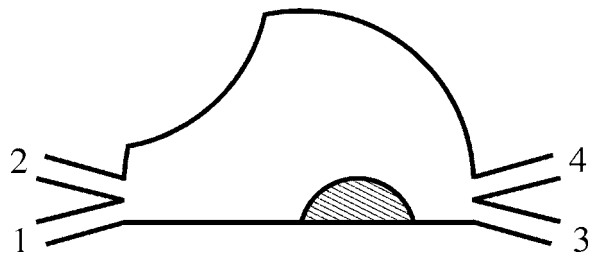

FIG. 1. Chaotic quantum dot entangler used in the numerical model. Leads connected to electron reservoirs support one orbital channel plus two spin channels each.

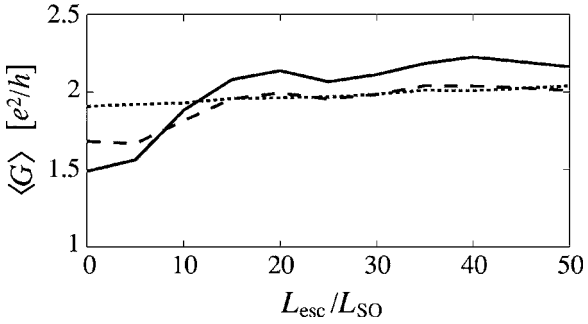

FIG. 2. Sample-averaged conductance $\langle G\rangle$ for the chaotic quantum dot of Fig. 1 vs SO coupling in the presence of a magnetic flux ϕ. The curves correspond to $\phi/\phi_0=0$ (solid line), 1/2 (dashed line), and 5 (dotted line). The results illustrate WL (WA) quantum corrections to the classical conductance ($2e^2/h$ in this case) for weak (large) SO coupling due to TRS ($\phi/\phi_0=0$). These quantum corrections disappear as TRS breaks ($\phi/\phi_0\neq 0$).

Two single-orbital-channel leads are attached at each side of the dot, similar to what was proposed in Ref. 2. In addition, each orbital mode can support two spin channels. The single-particle Hamiltonian for electrons with charge $-e$ and effective mass m^* reads

$$H=\frac{\mathbf{\Pi}^2}{2m^*}+\frac{\alpha_R}{\hbar}(\boldsymbol{\sigma}\times\mathbf{\Pi})_z+V(\mathbf{r}), \tag{1}$$

where $\mathbf{\Pi}=\mathbf{p}+(e/c)\mathbf{A}$, α_R is the Rashba SO coupling strength, $\boldsymbol{\sigma}$ is the vector of Pauli spin matrices, z is the axis perpendicular to the dot's plane, and V is a hard-wall confining potential describing the dot's contour. The strength of the Rashba SO interaction can be given in terms of the ratio L_{esc}/L_{SO}, where $L_{esc}=\pi A/w$ is the classical escape length in an open chaotic billard of area A with a total opening of width w,[29] and $L_{SO}=\pi\hbar^2/\alpha_R m^*$ is the spin-precession length due to SO coupling. A uniform magnetic field (generated by the vector potential $\mathbf{A}$) introduces a flux ϕ (measured in units of the flux quantum $\phi_0=hc/e$). Applying a (small) bias voltage between reservoirs produces a coherent electron current through the dot from left to right. For the calculation of the corresponding scattering amplitudes we implement a recursive Green's function technique based on a spin-dependent tight-binding model arising from a real-space discretization.[27] Additionally, we also perform some independent RMT simulations for comparison.

The single-particle transport properties are characterized by the Landauer-Büttiker linear conductance G. For illustration, in Fig. 2 we present some numerical results for the sample-average conductance $\langle G\rangle$ of the chaotic dot of Fig. 1 as a function of L_{esc}/L_{SO} and ϕ. Coherent backscattering leads to a minimum in G (WL) at $\phi=0$ in the absence of SO coupling. For large SO coupling, G presents a maximum (WA) instead. The transition from WL to WA shows up around $L_{esc}/L_{SO}\approx 10$ (see also Refs. 30–33). For a large ϕ, TRS is broken and G is independent of the SO coupling strength, remaining close to its classical value ($G_{cl}=2e^2/h$ in our case). Such underlying single-particle physics is relevant for the understanding of the two-particle effects reported in this paper. The crossover from WL to WA is also manifest, though differently, in the entanglement production as we see below.

III. ENTANGLEMENT PRODUCTION FROM SEPARABLE TWO-PARTICLE STATES

A. Incoming and outgoing two-particle states

We consider a separable two-particle state incoming from an electron reservoir on the left of the dot of Fig. 1:

$$|\Psi_{in}\rangle=a_1^{s_1\dagger}a_2^{s_2\dagger}|0\rangle, \tag{2}$$

where $a_i^{s_i\dagger}$ creates an incoming electron in lead $i=1,2$ with spin $s_i=\uparrow,\downarrow$, and $|0\rangle$ is the Fermi sea at zero temperature. Multiple scattering within the dot entangles the ougoing state. This is a coherent superposition of orbital and spin channels determined by the single-particle S matrix. It reads

$$|\Psi_{out}\rangle=\sum_{n,\sigma}\sum_{m,\tau}S_{n1}^{\sigma s_1}S_{m2}^{\tau s_2}b_n^{\sigma\dagger}b_m^{\tau\dagger}|0\rangle, \tag{3}$$

where $S_{ji}^{ss_i}$ is the scattering amplitude from lead $i=1,2$ with spin s_i to any lead $j=1,\ldots,4$ with spin s. The $b_j^{s\dagger}$ creates an outgoing electron in lead j with spin s, satisfying the vector equation $b^\dagger\cdot S=a^\dagger$. The terms in (3) with $n=m$, $\sigma=\tau$ vanish for the sake of fermionic statistics.

B. Particle conservation

The $|\Psi_{out}\rangle$ of Eq. (3) can be split into three terms with different local particle number at the left (n_L) and right (n_R) of the dot such that $n_L+n_R=2$, in the form

$$|\Psi_{out}\rangle=\sum_{n_L,n_R}|n_L,n_R\rangle=|2,0\rangle+|0,2\rangle+|1,1\rangle. \tag{4}$$

The accessible entanglement[34] in $|\Psi_{out}\rangle$ is studied in Bell-like measurements by performing local operations that conserve the local particle number.[1] This is of fundamental importance for electrons, preventing the local creation of states in a coherent superposition of different number of particles. This means that local operations do not mix the three terms of Eq. (4) and the entanglement can be studied in each of them independently.

C. The concurrence as an entanglement measure

We evaluate the amount of entanglement between pairs of two-level (sub)systems or qubits, which in our case correspond to an electron leaving the quantum dot in one of two predetermined orbital or spin states. This requires a bipartition of the system by choosing some pairs of outgoing channels of interest, tracing out the nonobserved degrees of freedom compatible with that choice. The two-qubit entanglement is quantified by the concurrence $0\leqslant C\leqslant 1$, defined as[35]

$$C(\rho)\equiv\max\{0,\lambda_1-\lambda_2-\lambda_3-\lambda_4\}. \tag{5}$$

The λ_i's are the square roots of the eigenvalues (in decreasing order) of the matrix $\rho\tilde{\rho}$, where $\rho\in 4\times 4$ is a two-qubit density matrix and $\tilde{\rho}\equiv(\sigma_y\otimes\sigma_y)\rho^*(\sigma_y\otimes\sigma_y)$, with σ_y the sec-

ond Pauli matrix. Separable unentangled states have $C=0$, while $C=1$ correspond to maximally entangled (Bell) states. States with $0<C<1$ are nonseparable, partly entangled states. A $C\neq 0$ is a necessary and sufficient condition for affirming that the two involved qubits are non-classically correlated due to entanglement. For electrons in the quantum dot of Fig. 1, where both orbital and spin degrees of freedom are involved, the two-particle density matrix ρ is generally larger than 4×4, i.e., it does not correspond to a two-qubit system. Still, a study of the, e.g., orbital qubits can be performed by defining a reduced density matrix (RDM) $\mathrm{Tr}_s(\rho)\in 4\times 4$, where the trace is taken over the spin degree of freedom s; and vice versa (see Sec. IV). For a chaotic dot, the outgoing wave function (3) is a function of a random scattering matrix S, and so its corresponding density matrix. The entanglement contained in (3) depends on the particular S, which is sample dependent. Hence, we characterize the production of entanglement in by calculating the sample-averaged $\langle C\rangle$ and its fluctuations $\mathrm{var}(C)\equiv\langle C^2\rangle-\langle C\rangle^2$. The concurrence can be related to zero-frequency current-noise measurements (i.e., without time-resolved detection) in mesoscopic conductors, as recently shown in Refs. 1 and 2. Alternatively, the presence of entanglement could be determined by other means such as, e.g., beam-splitter current correlations giving a lower bound for entanglement[36] or implementing some entanglement witness.[37] Here, we calculate C from its definition (5) for several bipartitions of the outgoing state (3) independently of any particular detection scheme.

IV. RESULTS

We investigate first the entanglement produced between outgoing left and right channels. To this aim we project $|\Psi_{\mathrm{out}}\rangle$ onto the subspace containing one single excitation at each side of the dot (i.e., $|1,1\rangle$). We obtain

$$|\Psi_{\mathrm{LR}}\rangle \equiv \sum_{p,\alpha}\sum_{q,\beta}(S^{\alpha s_1}_{p1}S^{\beta s_2}_{q2}-S^{\beta s_1}_{q1}S^{\alpha s_2}_{p2})b^{\alpha\dagger}_p b^{\beta\dagger}_q|0\rangle, \qquad (6)$$

where the indices $p=1,2$; $\alpha=\uparrow,\downarrow$ and $q=3,4$; $\beta=\uparrow,\downarrow$ stand for left and right outgoing channels, respectively. The density matrix of the state (6) reads $\rho_{\mathrm{LR}}=|\Psi_{\mathrm{LR}}\rangle\langle\Psi_{\mathrm{LR}}|/\langle\Psi_{\mathrm{LR}}|\Psi_{\mathrm{LR}}\rangle\in 8\times 8$, which by construction accounts for both orbital and spin degrees of freedom. The degree of orbital entanglement contained in (6) can be extracted from ρ_{LR} by tracing out the spin degree of freedom, defining the RDM $\rho^{\mathrm{orb}}_{\mathrm{LR}}=\sum_{\alpha,\beta}\langle\alpha,\beta|\rho_{\mathrm{LR}}|\alpha,\beta\rangle\in 4\times 4$ for two orbital qubits. Figure 3 shows results for the corresponding average concurrence $\langle C^{\mathrm{orb}}_{\mathrm{LR}}\rangle$ vs $L_{\mathrm{esc}}/L_{\mathrm{SO}}$ for parallel ($s_1=s_2=\uparrow$; solid line) and antiparallel ($s_1=\uparrow$, $s_2=\downarrow$; dashed line) incoming spins subject to a magnetic flux ϕ. The insets depict the fluctuations. Outgoing spins of different species do not contribute to orbital entanglement.[5] This is why only parallel incoming spins show a finite $\langle C^{\mathrm{orb}}_{\mathrm{LR}}\rangle\approx 0.39$ in the absence of SO coupling ($L_{\mathrm{esc}}/L_{\mathrm{SO}}=0$) when leaving the quantum dot. This value, almost unaffected by the breaking of TRS (finite ϕ), is in very good agreement with previous RMT results[2] depicted by the full dots in Fig. 3. As SO coupling increases, spins flip during transport and outgoing spin channels of different sign open up both at the left and right of the dot. This hinders the production of orbital entanglement from originally parallel spins, leading to a reduction of the concurrence. In contrast, for incoming antiparallel spins SO scattering contributes to the formation of orbitally entangled states between spins of the same outgoing species. The scale on which the concurrence varies significativelly as a function of $L_{\mathrm{esc}}/L_{\mathrm{SO}}$ is similar to that determining the transition fron WL to WA in the conductance shown in Fig. 2. For large SO coupling, the degree of entanglement saturates as the orientation of outgoing spins randomize. However, a finite difference $\Delta C\approx 0.05$ survives between different incoming spin configurations for $\phi=0$ (Fig. 3, upper panel). This is a consequence of the TRS correlations preserved by the SO interaction: As soon as a finite ϕ breaking TRS is applied the concurrence tends rapidly to a common asymptotic value independent of the initial condition (Fig. 3, lower panel). This indicates that breaking time-reversal and spin-rotation symmetries give rise to a residual orbital entanglement with universal average concurrence $\langle C^{\mathrm{orb}}_{\mathrm{LR}}\rangle\approx 0.075$ for chaotic dots. We point out that orbital entanglement is very sensitive to the spin dynamics even for broken TRS (Fig. 3, lower panel), where WL and WA quantum corrections to the conductance are absent (dotted line in Fig. 2; see also Refs. 30–33). Regarding the fluctuations (insets in Fig. 3), they show a functional dependence similar to that of the concurence. For large $L_{\mathrm{esc}}/L_{\mathrm{SO}}$, $\sqrt{\mathrm{var}(C)}\approx\langle C\rangle$. These features repeat in our results of Figs. 4 and 5. We further note that some difficulties may appear for detecting orbital entanglement produced from incoming antiparallel spins by violating Bell inequalities for shot noise as described in Ref. 2. This is because both incoming as well as outgoing channels would mix at the left side of the dot (unless they can be spatially separated). However, this does not exclude the possibility implementing alternative approaches

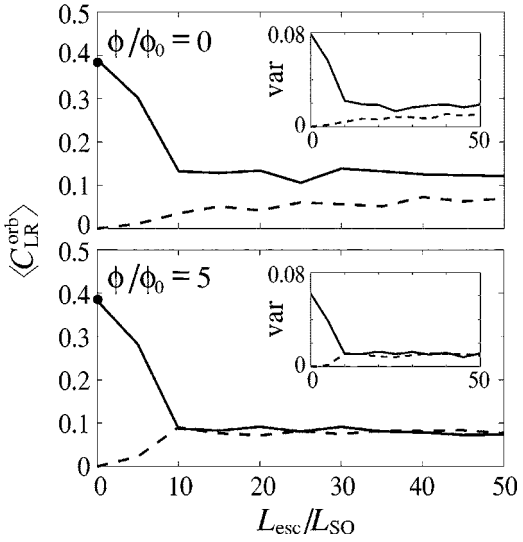

FIG. 3. Left-right orbital entanglement: $\langle C^{\mathrm{orb}}_{\mathrm{LR}}\rangle$ vs SO coupling with TRS preserved (upper panel) and broken (lower panel). Solid (dashed) lines correrspond to (anti)parallel incoming spins. Insets depict the fluctuations var(C), respectively. Full dots: RMT results from Ref. 2.

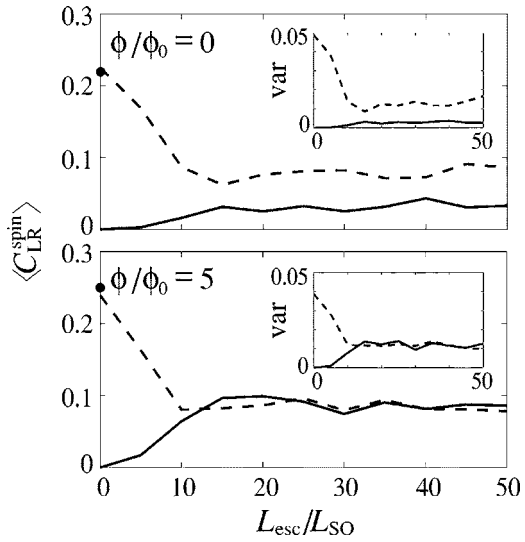

FIG. 4. Left-right spin entanglement: $\langle C_{LR}^{spin} \rangle$ vs SO coupling with TRS preserved (upper panel) and broken (lower panel). Solid (dashed) lines correrspond to (anti)parallel incoming spins. Fluctuations var(C) shown in insets. Full dots: RMT results.

for detection as, e.g., the determination of lower bounds for entanglement from beam-splitter current correlations[36] or the use of some entanglement witness.[37]

Information regarding the degree of spin entanglement between left and right channels contained in (6) can be evaluated from ρ_{LR} by tracing out the orbital degree of freedom instead, constructing the RDM $\rho_{LR}^{spin} = \Sigma_{p,q} \langle p,q | \rho_{LR} | p,q \rangle \in 4 \times 4$ for two spin qubits. Results for the corresponding average concurrence $\langle C_{LR}^{spin} \rangle$ are presented in Fig. 4. In contrast to the previous case of orbital entanglement, antiparallel incoming spins (dashed lines) lead now to a finite $\langle C_{LR}^{spin} \rangle$ already at $L_{esc}/L_{SO}=0$ due to exchange correlations, while parallel incoming spins (solid lines) do not.

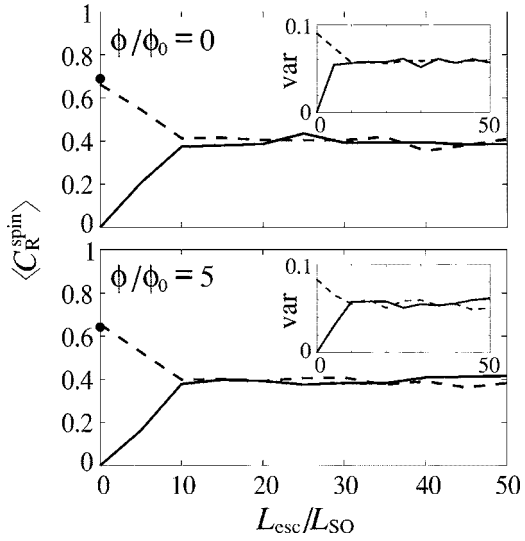

FIG. 5. Transmitted spin entanglement: $\langle C_{R}^{spin} \rangle$ vs. SO coupling with TRS preserved (upper panel) and broken (lower panel). Solid (dashed) lines correrspond to (anti)parallel incoming spins. Insets show the fluctuations var(C). Full dots: RMT results.

The result is in agreement with our independent RMT simulations (full dots) performed by following the approach of Ref. 2. The presence of multiple orbital channels give rise to an outgoing mixed state ($\mathrm{Tr}\, \rho_{LR}^{spin2} < 1$) with $\langle C_{LR}^{spin} \rangle < 1$. This differs from the case in which one single-orbital-channel lead is attached at each side of the dot: There, antiparallel incoming spins escape at the left and right in a pure singlet state with $\langle C_{LR}^{spin} \rangle = 1$ independently of the scattering amplitudes [straightfoward from Eq. (6); see also Ref. 5]. We also note that $\langle C_{LR}^{spin} \rangle \ll \langle C_{LR}^{orb} \rangle$ at $L_{esc}/L_{SO}=0$ (compare Figs. 3 and 4). This is probably related to the fact that, in contrast to spin entanglement, orbitally entangled electrons leave the dot at left and right in a pure state ($\mathrm{Tr}\, \rho_{LR}^{orb2} = 1$). For large SO coupling, Fig. 4 shows features similar to those for orbital entanglement: A finite ΔC survives between different incoming states at $\phi=0$ due to TRS correlations (Fig. 4, upper panel). The difference disappears as TRS is broken by a finite ϕ (Fig. 4, lower panel). More interestingly, the asypmtotic value for $\langle C_{LR}^{spin} \rangle$ is very similar to that for $\langle C_{LR}^{orb} \rangle$ in Fig. 3 (lower panel). This indicates the existence of a universal value for the concurrence of residual left-right entanglement independently of the initial condition *and* particular degree of freedom. The claim is supported by RMT, which shows that when both time-reversal and spin-rotation symmetries are broken the S matrix is uniformly distributed in the unitary group and no effective difference exists between spin and orbital channels.[38]

We consider now the entanglement production for transmitted spins, i.e., the spin entanglement between channels at the right side of the dot. This entanglement is contained in the $|0, 2\rangle$ component of Eq. (4). We note that such component splits at the same time into other three contributions, each of them with different local particle number at leads 3 (n_3) and 4 (n_4) such that $n_3+n_4=2$. Following Sec. III B, we see that also here the entanglement can be studied independently in each term due to local particle number conservation. The only component of interest is that one with one single excitation on each lead, obtained by projecting the outgoing state (3) onto the corresponding subspace. It reads

$$|\Psi_R\rangle \equiv \sum_{\alpha,\beta} (S_{31}^{\alpha s_1} S_{42}^{\beta s_2} - S_{41}^{\beta s_1} S_{32}^{\alpha s_2}) b_3^{\alpha\dagger} b_4^{\beta\dagger} |0\rangle, \qquad (7)$$

where α and β label ougoing spins in the leads 3 and 4, respectively. Note that the $|\Psi_R\rangle$ can be only spin entangled since there are just two orbital channels on the right side of the dot. After defining the density matrix $\rho_R^{spin} = |\Psi_R\rangle\langle\Psi_R| / \langle\Psi_R|\Psi_R\rangle$ for the two spin qubits, we plot in Fig. 5 (upper panel) the corresponding $\langle C_R^{spin} \rangle$ vs L_{esc}/L_{SO} for $\phi=0$. As in the previous case of left-right spin entanglement, only antiparallel incoming spins (dashed line) lead to a finite $\langle C_R^{spin} \rangle$ at $L_{esc}/L_{SO}=0$. However, the degree of entanglement is much larger (its value agrees with our RMT calculations depicted by the full dot). That holds true for large SO coupling, where the concurrence arrives at a relatively large common asymptotic value $\langle C_R^{spin} \rangle \approx 0.4$ independently of the initial condition. This contrast with our findings for left-right entanglement, where TRS correlations are relevant. The ap-

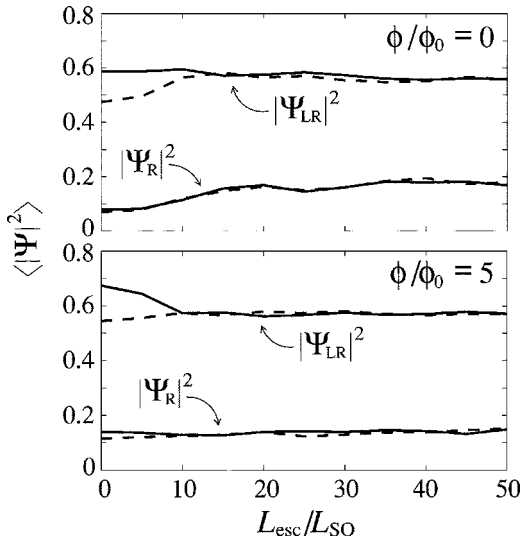

FIG. 6. Sample-averaged probabilities for the states (6) and (7) vs SO coupling. Left (right) panel shows results for preserved (broken) TRS. Solid (dashed) lines corrrespond to (anti) parallel incoming spins.

plication of a finite ϕ, Fig. 5 (lower panel), does not affect the zero-flux characteristics significatively.

Usefull information can be still extracted from the wave functions (6) and (7) by plotting their modulus square (Fig. 6). The larger contribution is given by $|\Psi_{LR}|^2$. The $|\Psi_R|^2$ is much smaller instead. It means that highly spin-entangled electrons transmitted to the right are actually produced with a lower probability. This can be understood by using classical probabilities in the limit of broken time-reversal and spin-rotation symmetries: The probability for the two incoming electrons to end up in any two different channels is 1/28. There are 16 combinations giving one electron on the left and one on the right, and only four with one electron in each lead 3 and 4. The quantities $16/28 \approx 0.571$ and $4/28 \approx 0.143$ are in agreement with the asymptotic values of Fig. 6 (lower panel). Quantum corrections to these values show up for small SO coupling, specially when $\phi=0$. We further note in Fig. 6 that a probability difference appears between parallel (solid line) and antiparallel (dashed line) incoming spins in the left-right component due to fermionic statistics. Breaking TRS increases the contribution, keeping the relative difference unaffected.

V. CONCLUSION

In summary, we studied the role of spin dynamics and TRS correlations in the production of entanglement in mesoscopic conductors and the connection with WL and WA quantum corrections. By including SO coupling, among other things we found that the TRS effects can be more important than originally thought.[2] These manifest both in the degree of entanglement as well as in the production rate. The effects of SO coupling appear on a scale corresponding to the pass from the regime of WL to WA in the quantum conductance. We also determined some universal characteristics of chaotic entanglers as the residual amount of entanglement produced after time-reversal and spin-rotation symmetry breaking.

ACKNOWLEDGMENTS

We thank C. W. J. Beenakker, M. Büttiker, M.-S. Choi, V. Giovannetti, and F. Taddei for useful comments. This work was supported by the European Commission through the Spintronics Research Training Network, and by the "Quantum Information" research program of Centro di Ricerca Matematica "Ennio de Giorgi" of Scuola Normale Superiore.

[1] C. W. J. Beenakker, in *Quantum Computers, Algorithms and Chaos*, Proceedings of the International School of Physics "Enrico Fermi," Varenna, 2005, (IOS Press, Amsterdam, 2006); cond-mat/0508488.
[2] C. W. J. Beenakker, M. Kindermann, C. M. Marcus, and A. Yacoby, in *Fundamental Problems of Mesoscopic Physics*, edited by I. V. Lerner, B. L. Altshuler, and Y. Gefen, NATO Science Series II vol. 154 (Kluwer, Dordrecht, 2004).
[3] C. W. J. Beenakker, C. Emary, M. Kindermann, and J. L. van Velsen, Phys. Rev. Lett. **91**, 147901 (2003).
[4] P. Samuelsson, E. V. Sukhorukov, and M. Büttiker, Phys. Rev. Lett. **92**, 026805 (2004).
[5] P. Samuelsson, E. V. Sukhorukov, and M. Büttiker, New J. Phys. **7**, 176 (2005).
[6] S. Bose and D. Home, Phys. Rev. Lett. **88**, 050401 (2002).
[7] A. I. Signal and U. Zülicke, Appl. Phys. Lett. **87**, 102102 (2005).
[8] A. V. Lebedev, G. B. Lesovik, and G. Blatter, Phys. Rev. B **71**, 045306 (2005).
[9] P. Recher, E. V. Sukhorukov, and D. Loss, Phys. Rev. B **63**, 165314 (2001).
[10] G. B. Lesovik, T. Martin, and G. Blatter, Eur. Phys. J. B **24**, 287 (2001).
[11] P. Samuelsson, E. V. Sukhorukov, and M. Büttiker, Phys. Rev. Lett. **91**, 157002 (2003); Phys. Rev. B **70**, 115330 (2004).
[12] P. Recher and D. Loss, Phys. Rev. B **65**, 165327 (2002); Phys. Rev. Lett. **91**, 267003 (2003).
[13] E. Prada and F. Sols, Eur. Phys. J. B **40**, 379 (2004); New J. Phys. **7**, 231 (2005).
[14] O. Sauret, D. Feinberg, and T. Martin, Phys. Rev. B **70**, 245313 (2004).
[15] C. Bena, S. Vishveshwara, L. Balents, and M. P. A. Fisher, Phys. Rev. Lett. **89**, 037901 (2002).
[16] V. Bouchiat, N. Chtchelkatchev, D. Feinberg, G. B. Lesovik, T. Martin, and J. Torres, Nanotechnology **14**, 77 (2003).
[17] W. D. Oliver, F. Yamaguchi, and Y. Yamamoto, Phys. Rev. Lett. **88**, 037901 (2002).
[18] D. S. Saraga and D. Loss, Phys. Rev. Lett. **90**, 166803 (2003).
[19] A. T. Costa and S. Bose, Phys. Rev. Lett. **87**, 277901 (2001).
[20] C. W. J. Beenakker and M. Kindermann, Phys. Rev. Lett. **92**, 056801 (2004).

[21] C. W. J. Beenakker, C. Emary, and M. Kindermann, Phys. Rev. B **69**, 115320 (2004).
[22] P. Samuelsson and M. Büttiker, Phys. Rev. B **71**, 245317 (2005).
[23] D. S. Saraga, B. L. Altshuler, D. Loss, and R. M. Westervelt, Phys. Rev. B **71**, 045338 (2005).
[24] L. Faoro, F. Taddei, and R. Fazio, Phys. Rev. B **69**, 125326 (2004).
[25] J. C. Egues, G. Burkard, D. S. Saraga, J. Schliemann, and D. Loss, Phys. Rev. B **72**, 235326 (2005).
[26] Y. Bychkov and E. Rashba, J. Phys. C **17**, 6039 (1984).
[27] For a detailed description of the numerical method see D. Frustaglia, M. Hentschel, and K. Richter, Phys. Rev. B **69**, 155327 (2004).
[28] Similar billiards were successfully used in the past for the numerical study of quantum corrections to the conductance of chaotic systems [see H. U. Baranger and P. A. Mello, Phys. Rev. Lett. **73**, 142 (1994)].
[29] See, e. g., K. Richter and M. Sieber, Phys. Rev. Lett. **89**, 206801 (2002).
[30] D. M. Zumbühl, J. B. Miller, C. M. Marcus, K. Campman, and A. C. Gossard, Phys. Rev. Lett. **89**, 276803 (2002).
[31] I. L. Aleiner and V. I. Fal'ko, Phys. Rev. Lett. **87**, 256801 (2001).
[32] P. W. Brouwer, J. N. H. J. Cremers, and B. I. Halperin, Phys. Rev. B **65**, 081302(R) (2002).
[33] O. Zaitsev, D. Frustaglia, and K. Richter, Phys. Rev. Lett. **94**, 026809 (2005); Phys. Rev. B **72**, 155325 (2005).
[34] H. M. Wiseman and J. A. Vaccaro, Phys. Rev. Lett. **91**, 097902 (2003).
[35] W. K. Wootters, Phys. Rev. Lett. **80**, 2245 (1998).
[36] G. Burkard and D. Loss, Phys. Rev. Lett. **91**, 087903 (2003); V. Giovannetti, D. Frustaglia, F. Taddei, and R. Fazio, Phys. Rev. B **74**, 115315 (2006).
[37] M. Horodecki, P. Horodecki, and R. Horodecki, Phys. Lett. A **223**, 1 (1996); M. Lewenstein, B. Kraus, J. I. Cirac, and P. Horodecki, Phys. Rev. A **62**, 052310 (2000).
[38] C. W. J. Beenakker, Rev. Mod. Phys. **69**, 731 (1997).